JOURNAL OF GEOPHYSICAL RESEARCH, VOL. 95, NO. B3, PAGES 2793–2809, MARCH 10, 1990

Dynamics of Degassing at Kilauea Volcano, Hawaii

SYLVIE VERGNIOLLE AND CLAUDE JAUPART

Laboratoire de Dynamique des Systèmes Géologiques, Université Paris 7 and Institut de Physique du Globe, Paris, France

At Kilauea volcano, Hawaii, the recent long-lived eruptions of Mauna Ulu and Pu'u O'o have occurred in two major stages, defining a characteristic eruptive pattern. The first stage consists of cyclic changes of activity between episodes of "fire fountaining" and periods of quiescence or effusion of vesicular lava. The second stage consists only of continuous effusion of lava. We suggest that these features reflect the dynamics of magma degassing in a chamber which empties into a narrow conduit. In the volcano chamber, gas bubbles rise through magma and accumulate at the roof in a foam layer. The foam flows toward the conduit, and its shape is determined by a dynamic balance between the input of bubbles from below and the output into the conduit. The foam thickness is proportional to $(\mu_l Q/\varepsilon^2 \rho_l g)^{1/4}$, where μ_l and ρ_l are the viscosity and density of magma, ε is the gas volume fraction in the foam, g is the acceleration of gravity, and Q is the gas flux. The bubbles in the foam deform under the action of buoyancy, and the maximum permissible foam thickness is $h_c = 2\sigma/\varepsilon\rho_l gR$, where σ is the coefficient of surface tension and R is the original bubble radius. If this critical thickness is reached, the foam collapses into a large gas pocket which erupts into the conduit. Foam accumulation then resumes, and a new cycle begins. The attainment of the foam collapse threshold requires a gas flux in excess of a critical value which depends on viscosity, surface tension, and bubble size. Hence two different eruption regimes are predicted: (1) alternating regimes of foam buildup and collapse leading to the periodic eruption of large gas volumes and (2) steady foam flow at the roof leading to continuous bubbly flow in the conduit. The essential result is that the continuous process of degassing can lead to discontinuous eruptive behavior. Data on eruption rates and repose times between fountaining phases from the 1969 Mauna Ulu and the 1983–1986 Pu'u O'o eruptions yield constraints on three key variables. The area of the chamber roof must be a few tens of square kilometers, with a minimum value of about 8 km^2. Magma reservoirs of similar dimensions are imaged by seismic attenuation tomography below the east rift zone. Close to the roof, the gas volume fraction is a few percent, and the gas bubbles have diameters lying between 0.1 and 0.6 mm. These estimates are close to the predictions of models for bubble nucleation and growth in basaltic melts, as well as to the observations on deep submarine basalts. The transition between cyclic and continuous activity occurs when the mass flux of gas becomes lower than a critical value of the order of 10^3 kg/s. In this model, changes of eruptive regime reflect changes in the amount and size of bubbles which reach the chamber roof.

1. INTRODUCTION

A volcano samples material from great depths in the Earth through a complex transport system. The best documented one is undoubtedly that of Kilauea on the island of Hawaii. Most studies of magma flow at depth have treated only the liquid phase, assuming implicitly that the volume of gas is negligible. Thus the deformation of the volcanic edifice has been used to calculate the rate at which new magma is introduced into the chamber or withdrawn from it [e.g., *Swanson*, 1972]. Eruptive phenomena suggest, however, that Kilauea volcano is not simply a passive conduit transferring magma from the mantle to the Earth's surface. It erupts in two major regimes: fire fountaining, where a powerful gas jet propels lava clots to heights of several hundred meters in the atmosphere, and effusion, where vesicular lava quietly oozes out of the vent. It may change regime from one eruption to the next and during the course of a single eruption. Previous models of eruption dynamics have emphasized the importance of volatile exsolution and expansion in the eruption conduits, i.e., in shallow parts of the system [*Wilson and Head*, 1981; *Head and Wilson*, 1987]. The volatile budget of Kilauea indicates, however, that magma already loses gas during storage at depth [*Gerlach and Graeber*, 1985; *Greenland*, 1989]. The purpose of the present study is to investigate the dynamics of this process and its influence on the eruption regimes.

At Kilauea, eruptions have occurred through different vents spread over a large area (Figure 1), and it seems difficult to conceive of a unique and simple framework within which to investigate their dynamics. However, recent long-lived eruptions have followed a characteristic eruptive pattern which provides crucial evidence for the processes at work in the plumbing system. Let us first refer to the 1969–1971 Mauna Ulu flank eruption [*Swanson et al.*, 1979]. In the initial stage, from June 1969 to January 1970, the same fissure alternated between phases of fire fountaining and effusive activity. A remarkable feature of this eruption stage was the variation of liquid level in the conduit: Once fire fountaining had stopped, the conduit appeared empty, and the top of the lava column could be found at a depth of 100 m or more. Eventually, lava would rise to the vent. From January 1970 until the end of the eruption in June 1971, fire fountaining was never observed again, and vesicular lava continuously issued from the fissure in the effusive regime. A phenomenon termed "gas piston" occurred in the conduit, such that lava followed a cycle of rise and fall associated with the ascent and bursting of a gas pocket. The Mauna Ulu eruption is particularly revealing because these various phenomena were observed on the same fissure. Other Hawaiian eruptions have shown the same phenomena in more complex conditions. The 1983–1988 Pu'u O'o flank eruption [*Wolfe et al.*, 1987] was similar to that of Mauna Ulu, except

Paper number 89JB03071.
0148-0227/90/89JB-03071$05.00

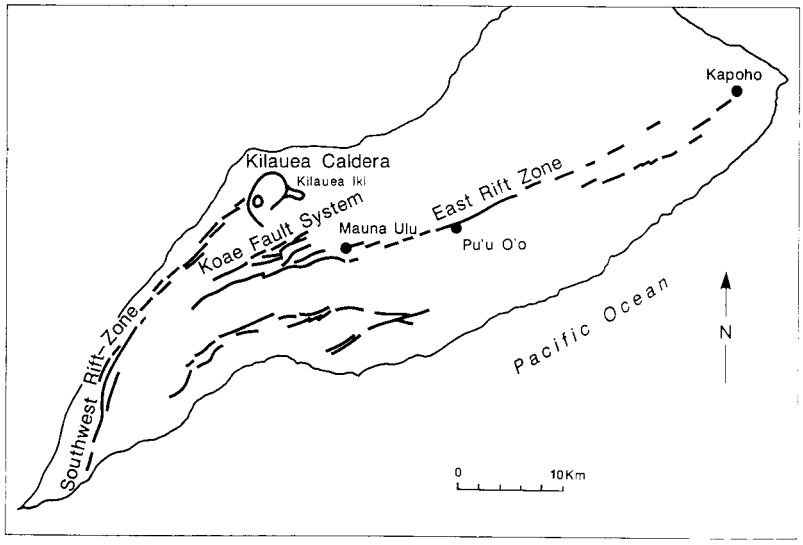

Fig. 1. Schematic map of Kilauea volcano showing major eruptive vents (adapted from *Wolfe et al.* [1987] and *Walker* [1988]). The three eruption sites to be discussed in this paper are identified by their local name: Kilauea Iki, Mauna Ulu, and Pu'u O'o.

that it was longer and that there was little effusive activity between two episodes of fire fountaining. It underwent the transition to continuous activity after about 3 years but out of a different fissure.

There is evidence that a CO_2 gas phase is present in the chamber which feeds the eruptions [*Gerlach and Graeber*, 1985; *Greenland et al.*, 1985; *Greenland*, 1989]. This free gas phase takes the form of gas bubbles which rise through magma, and we investigate what happens when the chamber empties into a conduit of smaller dimensions. Specifically, we apply our general experimental and theoretical results [*Jaupart and Vergniolle*, 1988, 1989] to the situation at Kilauea volcano in order to derive particular values for the area of the chamber roof, the gas volume fraction, and the bubble size in the chamber. We compare our results to field data in order to test the validity of the model. We end the paper with a detailed discussion of the applicability of the model and its implications for the interpretation of various volcanic phenomena.

2. The Model System

2.1. *Summary of Previous Studies*

The model relies on laboratory experiments and theory for a flat chamber roof described by *Jaupart and Vergniolle* [1988, 1989] (Figure 2). The basic principle is that gas bubbles rise through liquid and are trapped at the roof in a foam layer. Two phenomena affect the foam shape and thickness. One is the flux of bubbles from below, which acts to thicken the foam. The other is flow toward the conduit, which acts to thin the foam. An important variable is the mass flux of gas, which depends on the gas volume fraction and the bubble rise velocity. If it is sufficiently high, cyclic changes of activity are produced. The foam accumulates until it reaches a critical thickness and breaks down into a gas pocket which erupts violently (Figure 3). The cycle is repeated as a new foam layer builds up. The key fact is that the gas flux must exceed a critical value to achieve this.

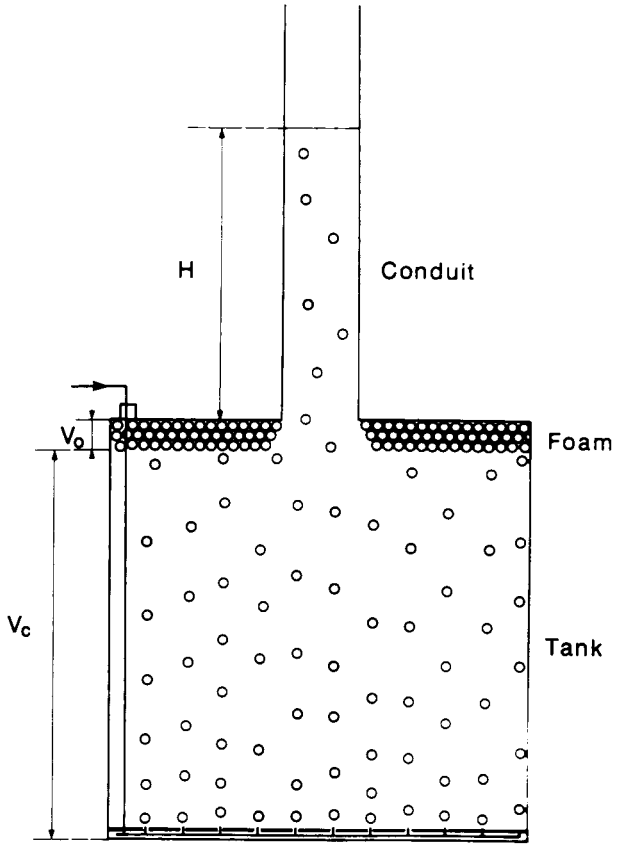

Fig. 2. Experimental setup to study the phenomena induced by degassing in a reservoir. Gas is injected through a set of capillary tubes at the bottom of a cylindrical tank. The height H of the liquid column in the conduit reflects the volume of gas contained in the system. This has two contributions: bubbles rising in the tank (V_c) and bubbles trapped in the foam layer at the roof (V_0). The gas volume fraction is α in the tank interior and ε in the foam at the roof, with typical values of 2 and 70%, respectively.

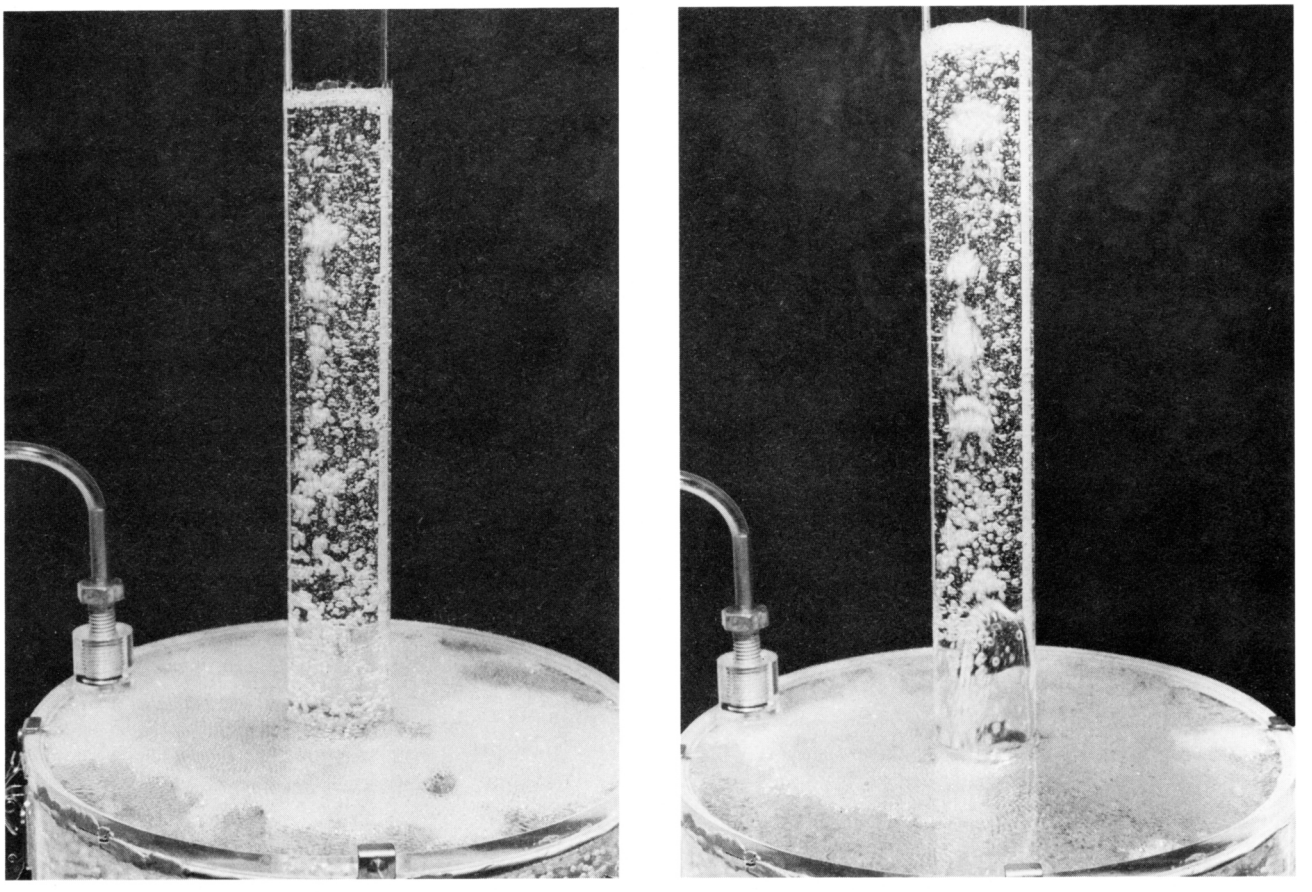

Fig. 3. The alternating regimes of foam build up and collapse [from *Jaupart and Vergniolle*, 1989]. From left to right and top to bottom. (*a*) The bubbles accumulate at the roof (white region) and liquid rises in the conduit. (*b*) At a critical thickness, the foam collapses into a single gas pocket which starts erupting. (*c*) The gas pockets erupts in an annular flow configuration with a central gas jet. (*d*) The gas pocket has erupted: note the liquid projections at the conduit walls and the drop of liquid level.

Below that value, continuous flow of a thin foam layer is observed. This is strongly reminiscent of the two main regimes of current Hawaiian eruptions described in the introduction, which will be called "cyclic" and "continuous" activity. The laboratory experiment also produces "gas piston" activity when minor coalescence events occur at the conduit edge as the foam flows.

The experiments are characterized by variations of liquid level in the conduit (Figures 2 and 3). As gas is fed into the tank bottom, liquid rises in the conduit to compensate for the gas volume contained in the tank. This gas volume is the sum of two contributions, one from the bubbles which rise through the tank and the other from the foam layer at the roof. For a given gas flux the former is constant, and hence cyclic changes of level reflect the buildup and collapse of the foam layer. Such changes have indeed been observed at Kilauea and had not been explained until this set of experiments.

The phenomena of bubble bursting and foam layer collapse are not instantaneous. Depending on the characteristic time for foam collapse, two situations arise [*Jaupart and Vergniolle*, 1989]. One is such that collapse is fast compared with the time taken by the foam to flow along the roof, implying that a single gas pocket is generated. In the other situation, collapse is long compared with the flow time, involving only parts of the foam before eruption into the conduit. In this case a number of gas pockets of small size are generated which rise and burst intermittently at the top of the liquid column. We have proposed that this situation reproduces the eruptive activity of Stromboli volcano (Eolian Islands). Here we focus on Hawaiian eruptions and hence on the first situation.

2.2. *Behavior of Bubbles in the Foam Layer*

The buoyant foam exerts a dynamic pressure ΔP in the thin liquid film which separates it from the roof. In the foam the bubbles are deformed and develop an approximately flat contact area S_1 against the roof (Figure 4). Consider a foam volume V_m with horizontal area S_m and thickness h where the gas volume fraction is ε. The total buoyancy force F is acting on n bubbles at the roof. Each bubble thus supports a force F/n, which is balanced by the excess pressure ΔP in the liquid film above it:

$$\frac{1}{n} V_m g(\rho_l - \rho_g)\varepsilon = \Delta P S_1 \tag{1}$$

Across the flat film, pressure is continuous, and gas inside the bubble is also with excess pressure ΔP. At the film edges this excess pressure is balanced by surface tension of the curved gas/liquid interface and hence

$$\Delta P = 2\sigma/r \tag{2}$$

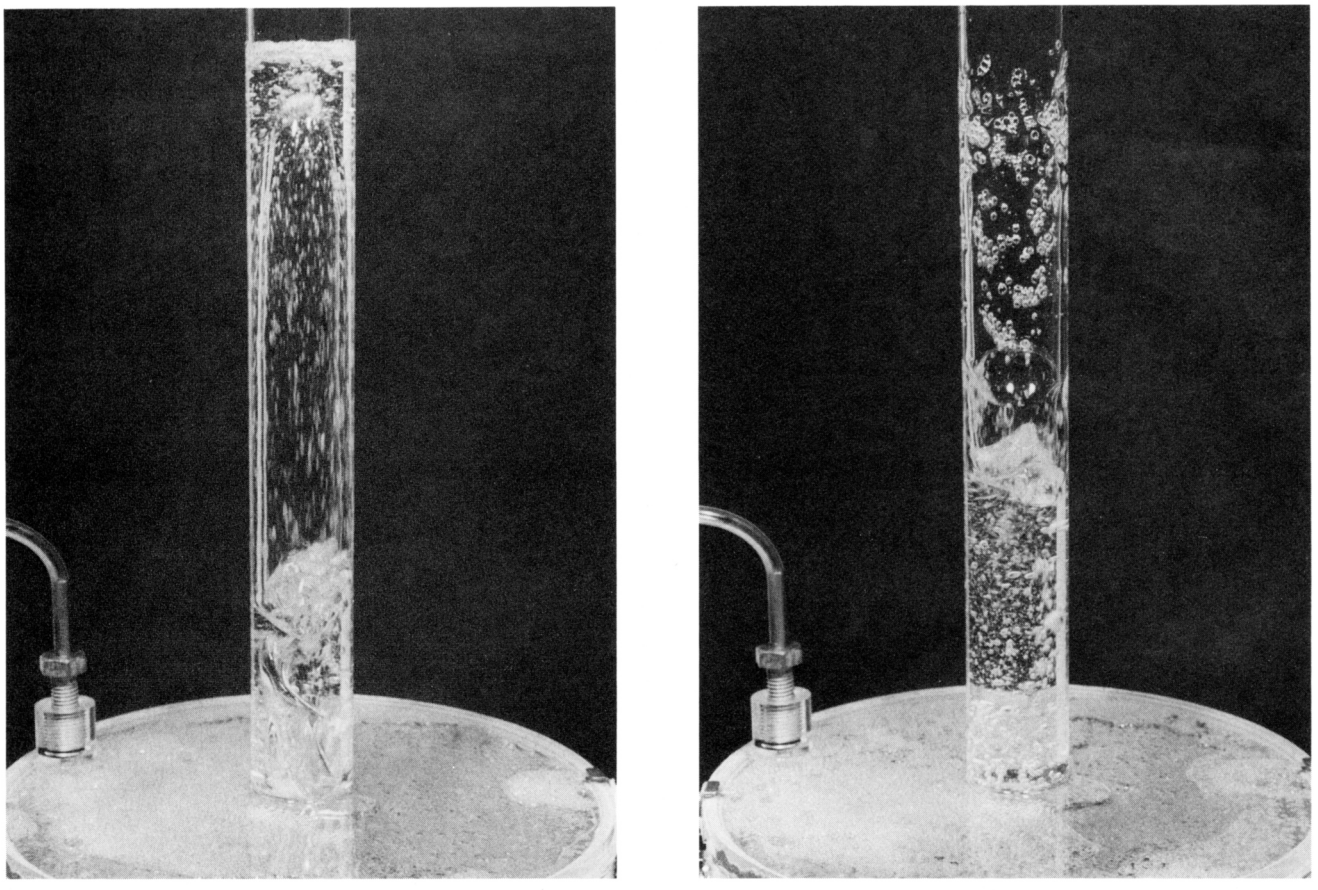

Fig. 3. (continued)

where σ is the coefficient of surface tension and r is the radius of curvature of the bubble close to the flat contact area (Figure 4). Each bubble occupies a cross-sectional area S_2 in the horizontal plane. Neglecting the small area occupied by liquid films between neighboring bubbles and the gas density, (1) and (2) are combined:

$$h = \frac{2\sigma}{\varepsilon \rho_l g} \frac{1}{r} \left(\frac{S_1}{S_2} \right) \tag{3}$$

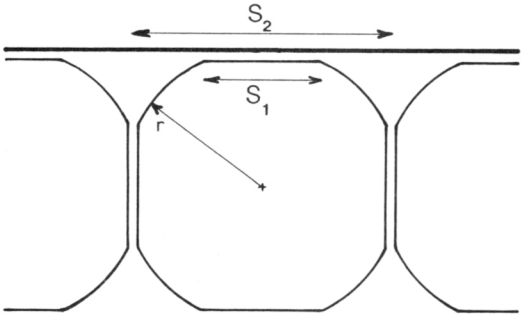

Fig. 4. Schematic representation of a bubble flattening against a rigid horizontal surface under its own buoyancy. S_1 is the contact area and r is the radius of curvature of the bubble walls just below. S_2 is the cross-sectional area occupied by the bubble in a horizontal plane. The liquid film above the bubble is thick enough so that molecular effects are negligible, and hence there is no "dispersive pressure" in the film [e.g., *Princen*, 1979].

In this problem, pressure variations are small and compression of the gas phase can be neglected. The bubbles are packed in the foam and hence are not free to deform independently of their neighbors. Specifying the geometrical characteristics of packing, it can be shown that r varies little and stays very close to the original bubble radius R [*Jaupart and Vergniolle*, 1989]. Thus (3) has the simple interpretation that as h increases, the bubble flattens such that the ratio of contact area to cross section increases. Maximum flattening is thus such that this ratio reaches the value of 1, which defines a critical thickness:

$$h_c = \frac{2\sigma}{\varepsilon \rho_l g} \frac{1}{R} \tag{4}$$

2.3. *Flow of Foam at the Roof*

The foam can be treated as a fluid with effective density and viscosity, ρ_m and μ_m respectively, [*Jaupart and Vergniolle*, 1989]:

$$\rho_m = (1 - \varepsilon)\rho_l + \varepsilon \rho_g \approx (1 - \varepsilon)\rho_l \tag{5a}$$

$$\mu_m = \mu_l (1 - \varepsilon)^{-5/2} \tag{5b}$$

where ρ_l and ρ_g are the densities of liquid and gas, μ_l is the liquid viscosity, and ε is the volume fraction of gas in the foam.

2.3.1. *Foam flow in a cylindrical tank.* We first investigate a cylindrical system with coordinates (r, z) (Figure 5).

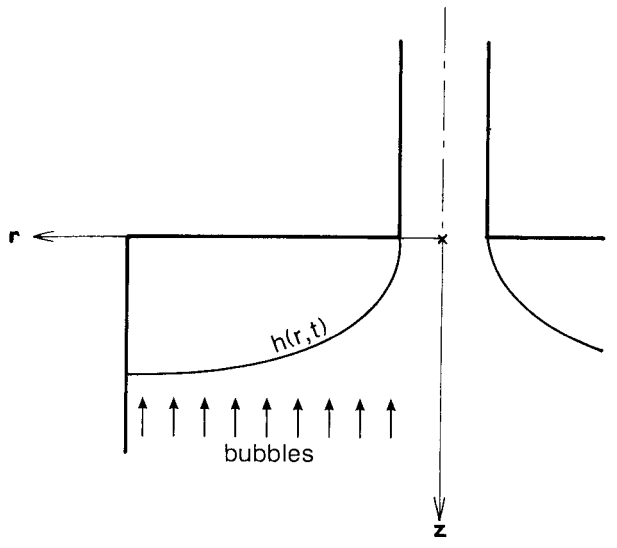

Fig. 5. Cylindrical coordinate system used to write down the equations for the flow of foam at the tank roof.

As it accumulates, the foam flows toward the conduit, behaving like a viscous current which is continuously fed from below. At radius r the foam thickness is $h(r, t)$, and the horizontal flux of foam is

$$\varphi(r, t) = 2\pi r \int_0^h u \, dz \tag{6a}$$

where u is the horizontal velocity. Conservation of mass requires

$$2\pi r \frac{\partial h}{\partial t} = 2\pi r q - \frac{\partial \varphi}{\partial r} \tag{6b}$$

where q is the vertical flux of foam due to the rising bubbles. If the total gas flux is Q, the corresponding flux of foam is $Q\varepsilon$, and q is equal to

$$q = Q/\varepsilon S_t \tag{7}$$

where S_t is the cross section of the tank.

The foam layer is thin compared to its horizontal dimensions, and hence a useful simplification to the equations of motion can be made using the "lubrication" approximation [*Batchelor*, 1967, p. 219]:

$$0 = -\frac{\partial P}{\partial z} + \rho_m g \tag{8a}$$

$$0 = -\frac{\partial P}{\partial r} + \mu_m \frac{\partial^2 u}{\partial z^2} \tag{8b}$$

Outside the foam the pressure distribution is hydrostatic. The amount of bubbles present is small (less than 2 vol % in our experiments) and hence

$$P(r, h, t) = P_{l0} + \rho_l g h \tag{9}$$

where P_{l0} is the pressure in the bulk liquid at depth $z = 0$ (at the conduit entrance). This allows the calculation of pressure within the foam, using (8a). Further, using the following boundary conditions

$$u(r, 0, t) = 0 \tag{10a}$$

$$\frac{\partial u}{\partial z}(r, h, t) = 0 \tag{10b}$$

the horizontal velocity field and hence the horizontal foam flux $\varphi(r, t)$ can be calculated. Substituting that expression in the continuity equation finally leads to the following equation for the foam height:

$$\frac{\partial h}{\partial t} = \frac{\varepsilon \rho_l g}{3\mu_m} \frac{1}{r} \frac{\partial}{\partial r}\left(r h^3 \frac{\partial h}{\partial r}\right) + q \tag{11}$$

This equation can be made dimensionless using the following scales:

$$r = r_t r' \tag{12a}$$

$$h = \{3\mu_m Q/\pi \varepsilon^2 \rho_l g\}^{1/4} h' \tag{12b}$$

$$t = \{3\pi^3 \mu_m \varepsilon^2/\rho_l g Q^3\}^{1/4} r_t^2 t' \tag{12c}$$

where r_t is the tank radius. At the tank periphery, there is no influx of bubbles into the foam layer, hence

$$\varphi(r_t, t) = 0 \tag{13a}$$

At the conduit edge the lubrication approximation fails as foam flow becomes vertical. For the purposes of computing the foam thickness at a finite distance from the conduit it is sufficient to use the following boundary condition [*Beckett and Poots*, 1975]:

$$h(r_c, t) = 0 \tag{13b}$$

where r_c is the conduit radius. Despite this condition the flux of foam remains finite because it is proportional to $\partial(h^4)/\partial r$ and not simply to h (Appendix A).

With the obvious initial condition $h(r, 0) = 0$ the solution can be found by numerical integration. The behavior of the foam layer can be described as follows (Figure 6a). Flow into the conduit is driven by variations of foam thickness and develops with time as the foam accumulates: It is initially confined to the vicinity of the conduit and propagates radially outward to affect increasingly larger portions of the foam (Figure 6a). Thus for short times and away from the conduit the foam layer is flat, and its thickness increases linearly with time in response to the constant input of bubbles from below (Figure 6b). For longer times the foam adopts a steady state shape, such that flow into the conduit balances this input. Therefore for a given gas flux there is a maximum foam thickness which is the steady state value at the tank periphery:

$$h_m = \left\{\frac{\mu_m Q}{\varepsilon^2 \rho_l g}\right\}^{1/4} \left\{\frac{3}{\pi}\left[\ln\left(\frac{S_t}{S_c}\right) + \frac{S_c}{S_t} - 1\right]\right\}^{1/4} \tag{14}$$

where we have used the tank and conduit cross sections S_t and S_c. The important result is that this thickness increases with the gas flux Q.

2.3.2. *Elongated rectangular tank.* To evaluate the importance of the system geometry, we now look at the two-dimensional problem in (x, z) coordinates, which is

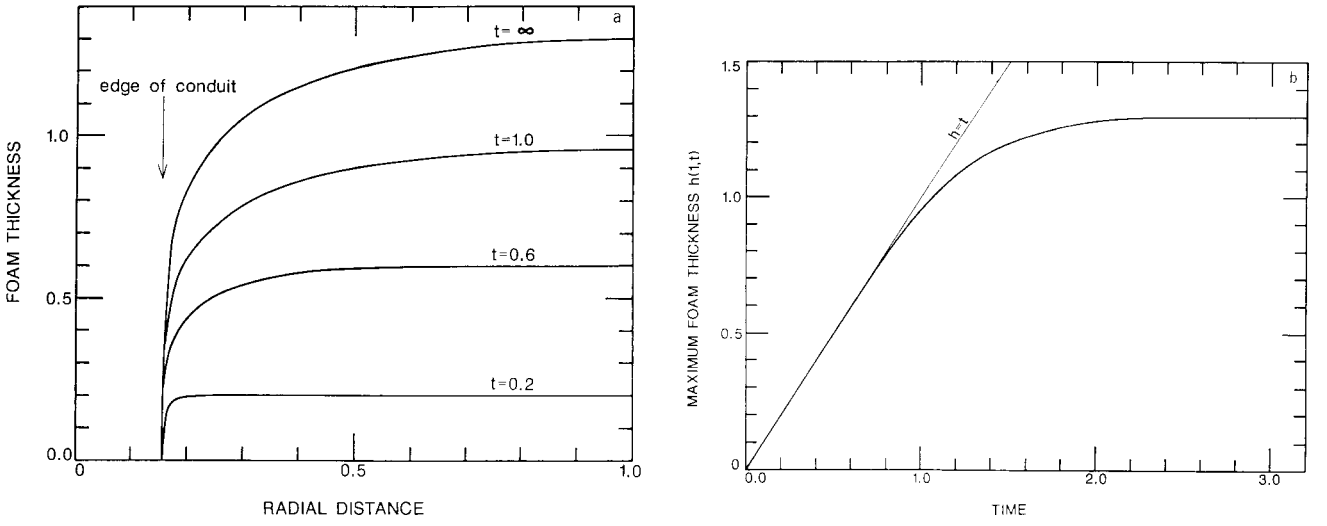

Fig. 6. (*a*) Foam thickness as a function of radial distance for three different times and at steady state, in nondimensional variables. In the laboratory experiments the dimensionless conduit radius is 0.157. (*b*) Foam thickness at the tank periphery $h(1, t)$ as a function of time in nondimensional variables. For small times it increases as t due to the constant flux of bubbles from below and because it is not affected by flow into the conduit.

appropriate for an elongated chamber emptying into a fissure. A rectangular chamber is topped in the middle by a narrow slit at $x = 0$. Its length is $2L$ in the x direction, and its dimension Δ in the y direction is much larger than L. The foam thickness $h(x, t)$ is now given by

$$\frac{\partial h}{\partial t} - \frac{\varepsilon \rho_l g}{3\mu_m} \frac{\partial}{\partial x}\left(h^3 \frac{\partial h}{\partial x}\right) = q \tag{15}$$

where all symbols are the same as before. The reservoir cross section is $S_t = 2L\Delta$, and the gas flux Q is such that

$$q = Q/\varepsilon 2L\Delta \tag{16}$$

The maximum foam thickness at a given gas flux Q is

$$h_m = \left\{\frac{\mu_m Q}{\varepsilon^2 \rho_l g}\right\}^{1/4} \left\{\frac{3}{2}\frac{S_t}{\Delta^2}\right\}^{1/4} \tag{17}$$

2.4. *Foam Collapse*

Above the critical thickness h_c, no equilibrium shape is possible for the bubbles at the roof. Thus the condition for collapse is that the foam reaches that critical thickness. At low gas flux the foam is thinner than h_c and hence is stable, which results in steady foam flow. If the gas flux increases, so does the foam thickness. The smallest gas flux Q_c for which the foam reaches the critical thickness is such that

$$h_m = h_c \tag{18}$$

or using (14) and (17),

$$A\{Q_c \mu_m/\varepsilon^2 \rho_l g\}^{1/4} = 2\sigma/\varepsilon \rho_l g R \tag{19}$$

where A is a constant which depends on the roof area and geometry. Using (5*b*) for the foam viscosity, we obtain

$$Q_c = \left\{\frac{4}{A}\right\}^4 \frac{1}{g^3} \frac{(1-\varepsilon)^{5/2}}{\varepsilon^2} \frac{\sigma^4}{\rho_l^3 \mu_l d^4} \tag{20}$$

where the bubble diameter d has been used instead of radius R.

At the critical gas flux Q_c the foam layer is at steady state, and its thickness is equal to the critical value over a small area at the tank periphery. This implies that only a small part of the foam collapses and hence that a small gas pocket forms. At a higher gas flux the foam reaches the critical thickness before steady state. Its thickness has the critical value over an annulus between the tank periphery and some intermediate radius, and collapse affects all this region. Therefore the volume of the gas pocket increases as the gas flux increases. The maximum volume corresponds to a foam with thickness h_c everywhere. Neglecting the small cross section of the conduit, this is equal to

$$V_p = \varepsilon S_t h_c \tag{21}$$

This volume is obtained at high values of the gas flux, such that the foam thickness grows proportional to time and to flux q (Figure 6*b*). Thus the critical time t_c needed to reach thickness h_c is given by

$$qt_c = h_c \tag{22}$$

Laboratory measurements of the critical gas flux, the erupted volume, and the critical time t_c are in agreement with the predictions of (20), (21), and (22) [*Jaupart and Vergniolle*, 1989].

3. CHARACTERISTICS OF KILAUEAN ERUPTIONS

3.1. *Magma Transport System of Kilauea Volcano*

The locations of the many earthquakes which occur within the volcanic edifice have been used to delineate the magma transport system [*Koyanagi et al.*, 1976; *Ryan et al.*, 1981; *Klein et al.*, 1987]. However, some of these earthquakes may not be related to fluid movements. Below the summit caldera (Figure 1), both the lack of seismicity and low seismic

velocities suggest the presence of a magma reservoir [*Thurber*, 1987]. A common interpretation is that this reservoir is rather small, a few kilometers in width and length and that it generates dikes which feed flank fissures along the east rift zone several tens of kilometers away. This view may be oversimplified. *Casadevall and Dzurisin* [1987] and *Walker* [1988] have drawn attention to the fact that there are remarkably few dikes exposed in the walls of Kilauea caldera and that the east rift zone is cut obliquely by the fissure directions. Detailed geodetic measurements around the Pu'u O'o fissure show that the feeder dike is of limited horizontal extent and cannot be traced back to the summit [*Hoffman*, 1988]. *Swanson et al.* [1976] and *Walker* [1988] have argued that there must be a fluid core which connects the Kilauea summit chamber to the east rift zone. Indeed, high-resolution attenuation tomography (P. Ho-Liu et al., Three-dimensional attenuation structure of Kilauea east rift zone, Hawaii, submitted to *Journal of Geophysical Research*, 1989, hereinafter referred to as submitted manuscript, 1989) reveals the presence of an elongated magma reservoir of large dimensions at a depth of about 4 km in this area conspicuous for its lack of seismicity [*Ryan*, 1988]. Small local magma reservoirs are also imaged at depths of about 2 km below recent eruption sites such as Pu'u O'o (P. Ho-Liu et al., submitted manuscript, 1989).

The distribution and chronology of events during a single eruptive event are complex. For example, during January 1983, just as the Pu'u O'o eruption was starting, swarms of earthquakes occurred along the east rift zone, together with inflation. They initially indicated downrift migration, i.e., eastward, but later showed uprift migration [*Koyanagi et al.*, 1989]. An intriguing feature is the existence of aseismic regions, either laterally in isolated segments along the rift or vertically within the 3- to 5-km depth range [*Wolfe et al.*, 1987; *Koyanagi et al.*, 1989]. One interpretation is that the earthquakes mark the tip of a large horizontal dike which propagated from the summit region toward the east, encountering small isolated magma bodies along the way. This interpretation does not explain the apparent reversal in the direction of earthquake migration. Further, the dike tip must have extended over the 3- to 5-km depth range where there was no seismicity, and it is difficult to see why it should not induce fracturing there as well. We conclude that the exact path followed by magma remains open to question and may include the deep storage reservoir which underlies a large part of the east rift zone.

3.2. *Chemistry of Lava and Volcanic Gases*

In general, magma is along "the olivine control line," which means that it has been affected by variable amounts of fractional crystallization [*Wright et al.*, 1975; *Garcia and Wolfe*, 1989]. This implies storage at depth prior to eruption. In detail, the compositional trends of erupted lava are complex and suggest that the reservoir is zoned.

Volcanic gases sampled during eruption in the east rift zone contain about 80–85% H_2O and 2–3% CO_2 by volume [*Gerlach and Graeber*, 1985; *Greenland*, 1989]. Their C/S atomic ratio is low in contrast to most basaltic gases [*Gerlach*, 1982] and further remains constant regardless of variable water contents [*Greenland*, 1987, 1989]. This suggests that the amounts of H_2O and CO_2 are not controlled by the same processes. Sustained summit eruptions, which are believed to reflect direct magma transport from the mantle source, involve gases which are significantly richer in CO_2 [*Gerlach and Graeber*, 1985]. Estimates for the composition of the "parental" magma which enters Kilauea volcano, based upon data from glass inclusions in olivine phenocrysts [*Harris and Anderson*, 1983] are 0.3 wt % H_2O and 0.6 wt % CO_2 [*Gerlach and Graeber*, 1985]. At pressures of 5×10^7–10^8 bars, which characterize the shallow plumbing system of Kilauea, the solubility of CO_2 in basalt ranges from 0.02 to 0.04 wt % [*Stolper and Holloway*, 1988]. These values indicate that a CO_2 gas phase is present at depth. Thus *Gerlach and Graeber* [1985] and *Greenland* [1989] propose that magma loses CO_2 during storage in the edifice but only exsolves H_2O close to the surface during active eruption.

Gas monitoring entails two difficulties. One is that given that deformation and magma flow processes are discontinuous, a mass budget for both gas and magma requires specific assumptions on the degassing process. As suggested by the present analysis, degassing can be continuous at depth, i.e., bubbles rising through a large magma reservoir, and discontinuous in the conduit. The other is that no direct measurement of gas composition is available for active fire fountains owing to sampling difficulties and large oxidization effects [*Greenland*, 1989]. Yet, as we shall show, fire fountains issue very large amounts of gas.

3.3. *Volume of Gas Erupted During Fire Fountaining*

We use data from the 1969–1971 Mauna Ulu [*Swanson et al.*, 1979] and the 1983–1989 Pu'u O'o [*Wolfe et al.*, 1987] flank eruptions. During their first stage of cyclic activity, they shared similar characteristics. Fire fountains had heights from several tens of meters to a maximum of about 500 m and lasted several hours: from 4 to 9 hours at Mauna Ulu and from 4 to 30 hours at Pu'u O'o. These similarities argue for the operation of the same mechanism in a system of similar dimensions. Knowing the fountain height z_m, it is possible to calculate approximately the exit velocity through ballistics [*Wilson*, 1980]:

$$v = (2gz_m)^{1/2} \tag{23}$$

During fire fountaining, lava makes up less than 1% of the volume erupted (*Vergniolle and Jaupart* [1986]; see also below). Hence the volume of gas erupted can be calculated directly by multiplying the exit velocity by the vent cross section and the duration. For Pu'u O'o we did not use data from the first three phases because the length of the active fissure changed rapidly. In later phases the fissure cross section remained close to 300 m^2, and the fountain height was monitored continuously (Hawaiian Volcano Observatory data, 1983–1986, courtesy of C. Heliker and G. Ulrich). In the Mauna Ulu eruption the fissure cross section varied from about 1000 to 250 m^2. Only the maximum fountain height for each episode was recorded [*Swanson et al.*, 1979], implying that the calculations are less accurate. Figure 7 shows the gas volume erupted in each fountaining phase at Pu'u O'o. The data exhibit fluctuations, but there is a clear trend of decreasing volume as time increases. We find that the volumes take a restricted and similar range of values: from 4×10^8 to 3×10^9 m^3 at Pu'u O'o and from 2×10^8 to 2.6×10^9 m^3 at Mauna Ulu.

These gas volumes are compared with those of erupted

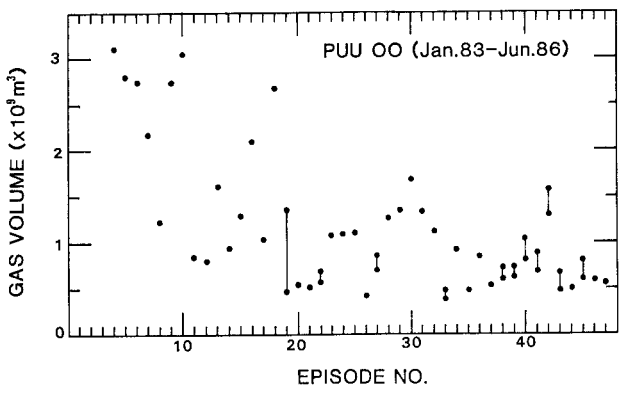

Fig. 7. Volume of gas erupted by fire fountaining during the 1983–1986 Pu'u O'o eruption (Hawaiian Volcano Observatory data, 1983–1986, courtesy of C. Heliker and G. Ulrich). Vertical bars indicate two extreme estimates in cases where the fountain height could not be measured continuously because of unfavorable weather conditions. Note the trend toward lower values as the eruption proceeds.

lava in Table 1. The erupting mixture is almost pure gas, lava usually making up less than 0.5% of the total volume. To calculate the corresponding mass proportions, the composition of the gas phase must be specified. Following *Gerlach and Graeber* [1985] and *Greenland* [1989], we first assume that the gas contains 85% H_2O and 2% CO_2 by volume and find that water may represent as much as 2% by weight of the erupted lava. This is much higher than the estimated values given in section 3.2. We also tried the composition of gases from sustained summit eruptions (37% H_2O and 49% CO_2 by volume according to *Gerlach and Graeber* [1985]). For example, taking CO_2, we find that it commonly represents more than 2% by weight of the erupted lava, which is again much too high. These calculations indicate that gas accumulation takes place at depth, which agrees with our conceptual model.

Interestingly, the gas/lava mass ratio decreases as the eruption proceeds and tends toward values characteristic of "parental" melt (Table 1). It is worth emphasizing, however, that these ratios do not represent actual values for the mixture which leaves the chamber. One reason is that part of the erupted magma was stored in the conduit itself. The other reason is that flow is separated, which implies that it is the mass flux ratio which is conserved and not the mass ratio. This is a property not only of the present model but also of basaltic eruptions in general [*Vergniolle and Jaupart*, 1986].

3.4. *The 1959 Kilauea Iki Eruption*

This eruption had many episodes of fire fountaining through a summit vent, with similar characteristics to those at Mauna Ulu and Pu'u O'o. This shows that cyclic changes of activity are not a feature only of flank eruptions in the east rift zone. An interesting feature of this eruption is that it occurred in the summit crater and formed a lava lake, where all erupted lava was stored. After the fourth fountaining episode the lava lake reached a constant level, and there was no net volume increase of lava. Yet more than 10 phases of cyclic activity occurred in which the level of the lake rose, only to return to its initial value by backflow of lava down the vent. This striking observation is consistent with the eruption of a gas pocket which is lost to the atmosphere but contributes no addition of lava to the surface. In fact, this sequence of events is identical to that of our laboratory experiments (Figure 3), with the caldera acting as the upper part of our conduit.

4. QUANTITATIVE ANALYSIS

We now apply our model to the data of Table 1 to obtain values for the area of the chamber roof and the size of gas bubbles.

4.1. *Physical Properties of Kilauean Basalt*

For viscosity (see Table 2) we take the compositions of the Mauna Ulu lavas given by *Wright et al.* [1975] and the empirical relationship of *Urbain et al.* [1982] for a temperature of 1200°C. We find values of about 30 Pa s which depend on the exact composition chosen. Direct measurements on samples from the Makaopuhi lava lake by *Shaw et al.* [1968] indicate a slightly higher value of 50 Pa s at that same temperature due to a composition difference. For surface tension, three independent studies on basaltic melts give values between 0.36 and 0.40 kg s^{-2} at atmospheric pressure and at a temperature of 1200°C [*Murase and McBirney*, 1973; *Khitarov et al.*, 1979; *Walker and Mullins*, 1981]. At atmospheric pressure, surface tension is weakly sensitive to temperature and the compositions of either the melt or the gas phase. Surface tension decreases with increasing pressure at a rate which depends strongly on the gas composition [*Khitarov et al.*, 1979]. In a pure water atmosphere it drops to a value of 0.1 kg s^{-2} at 5 kbar. In the present case the relevant pressure is that at the roof, which must be less than 1 kbar. We take a value of 0.3 kg s^{-2}, which cannot be wrong by more than 20%.

4.2. *Volume of the Gas Pocket*

We have shown that during fire fountaining, there is little lava in the mixture which rises in the conduit. Taking the estimated concentrations of 0.30 wt % H_2O and 0.03 wt % CO_2 for magma which leaves the chamber [*Gerlach and Graeber*, 1985; *Greenland*, 1989], we can calculate the mass of gas which can be exsolved from the erupted lava. We find that it represents initially a small fraction of the total amount of gas in the fountain (Table 1). In our model, fire fountaining is driven by a large gas pocket, and hence we take the mass of gas erupted to be equal to that of the pocket. To calculate the corresponding volume, we must account for the effect of pressure. The chamber roof is at a depth between 2 and 5 km and hence at a pressure between about 5×10^7 and 10^8 Pa. For these pressures it is appropriate to use the perfect gas equation of state. At a pressure of 5×10^7 Pa the volume of gas was between 8×10^5 and 6×10^6 m^3 in the Pu'u O'o case.

The amount of gas in the pocket is not always equal to that trapped in the whole foam because of two phenomena observed in the laboratory: one is that the gas pocket does not always escape in one piece, and the other that collapse does not always affect the whole foam. These also seem to occur in the field. For example, the twelfth phase of fountaining at Mauna Ulu was unusually short and followed 4 hours later by a stronger phase with more typical character-

TABLE 1. Amount of Lava and Gas Erupted During Fire Fountains at Pu'u O'o

Episode	Dense Lava Volume,* $\times 10^6$ m^3	Lava Mass, $\times 10^9$ kg	Water Mass Exsolved From Lava,† $\times 10^7$ kg	Gas Volume in Fountain, $\times 10^9$ m^3	Lava Volume in Fountain, wt %	H_2O Contents for East Rift Composition‡		CO_2 Contents for "Sustained Summit" Composition§	
						Mass Erupted, $\times 10^8$ kg	Weight Percent in Lava	Mass Erupted, $\times 10^8$ kg	Weight Percent in Lava
4	8.3	21.5	6.9	3.1	0.3	3.9	1.8	5.8	2.7
5	9.8	25.4	8.1	2.8	0.3	3.6	1.4	5.3	2.1
6	6.8	17.6	5.6	2.8	0.2	3.5	2.0	5.2	3.0
7	10.5	27.3	8.7	2.2	0.5	2.8	1.0	4.1	1.5
8	6.0	15.6	5.0	1.2	0.5	1.6	1.0	2.3	1.5
9	6.0	15.6	5.0	2.7	0.2	3.5	2.2	5.2	3.3
10	10.5	27.3	8.7	3.1	0.3	3.9	1.4	5.8	2.1
11	9.0	23.4	7.5	0.8	1.0	1.1	0.5	1.6	0.7
12	6.0	15.6	5.0	1.0	0.6	1.2	0.8	1.8	1.2
13	7.5	19.5	6.2	1.6	0.5	2.1	1.1	3.1	1.6
14	4.5	11.7	3.7	0.9	0.5	1.2	1.0	1.8	1.5
15	6.0	15.6	5.0	1.3	0.5	1.7	1.1	2.5	1.6
16	9.0	23.4	7.5	2.1	0.4	2.7	1.1	4.0	1.7
17	7.5	19.5	6.2	1.1	0.7	1.3	0.7	2.0	1.0
18	18.0	46.8	15.0	2.7	0.7	3.4	0.7	5.1	1.1
19	1.5	3.9	1.2	1.4	0.1	2.3	4.4	3.5	6.5
20	3.0	7.8	2.5	0.6	0.5	0.7	0.9	1.0	1.3
21	4.3	11.1	3.6	0.5	0.8	0.7	0.6	1.0	0.9
22	5.8	15.0	4.8	0.6	0.9	0.8	0.5	1.2	0.8
23	7.1	18.5	5.9	1.1	0.6	1.4	0.8	2.1	1.1
24	8.7	22.6	7.2	1.1	0.8	1.4	0.6	2.1	0.9
25	8.3	21.6	6.9	1.1	0.7	1.4	0.7	2.1	1.0
26	5.0	12.9	4.1	0.4	1.2	0.5	0.4	0.8	0.6
27	6.3	16.4	5.2	0.7	0.9	0.9	0.6	1.3	0.8
28	9.3	24.2	7.7	1.3	0.7	1.6	0.7	2.4	1.0
29	9.8	25.4	8.1	1.3	0.7	1.7	0.7	2.6	1.0
30	10.6	27.5	8.8	1.7	0.6	2.1	0.8	3.2	1.2
31	14.6	37.8	12.1	1.3	1.1	1.7	0.5	2.6	0.7
32	12.2	31.8	10.2	0.8	1.6	1.0	0.3	1.5	0.5
33	5.9	15.4	4.9	0.4	1.5	0.5	0.3	0.7	0.5
34	8.0	20.7	6.6	0.9	0.9	1.2	0.6	1.8	0.8
35	8.8	22.8	7.3	0.5	1.7	0.6	0.3	0.9	0.4
36	8.6	22.4	7.2	0.9	1.0	1.1	0.5	1.6	0.7
37	11.0	28.7	9.2	0.5	2.0	0.7	0.2	1.0	0.4
38	11.1	28.9	9.2	0.6	1.8	0.8	0.3	1.1	0.4
39	10.3	26.7	8.5	0.7	1.5	0.9	0.3	1.3	0.5
40	8.3	21.5	6.9	0.8	1.0	1.0	0.5	1.5	0.7
41	9.8	25.4	8.1	0.7	1.4	0.9	0.4	1.3	0.5
42	9.0	23.4	7.5	1.3	0.7	1.6	0.7	2.4	1.0
43	7.5	19.5	6.2	1.2	1.1	1.5	0.4	2.2	0.7
44	7.5	19.5	6.2	0.5	1.4	0.7	0.3	1.0	0.5
45	6.0	15.6	5.0	1.4	0.7	1.8	0.7	2.7	1.0
46	6.0	15.6	5.0	0.6	1.0	0.8	0.5	1.1	0.7
47	6.8	17.6	5.6	0.6	1.2	0.7	0.4	1.1	0.6

*Corrected for 25% vesicularity.
†For 0.32 wt % in magma composition [*Gerlach and Graeber*, 1985; *Greenland*, 1989].
‡Using the composition of volcanic gases on the east rift zone (85 vol % H_2O) [*Gerlach and Graeber*, 1985; *Greenland*, 1989].
§Using the composition of volcanic gases during sustained summit eruption (50 vol % CO_2) [*Gerlach and Graeber*, 1985; *Greenland*, 1989].

istics; *Swanson et al.* [1979] raised doubts about whether or not these two phases were distinct. Some of the variations shown in Figure 7 may be attributed to these effects.

4.3. *Gas Flux From the Chamber Interior*

Figure 8 shows the repose times for the Pu'u O'o eruption. A fountaining episode expels a gas volume V_2, which has been accumulated in the repose time t_{1-2} which preceded it. However, the ratio between these two quantities provides an estimate only of the accumulation rate of gas at the roof and not of the total gas flux. The reason for this is that as the foam accumulates at the roof, it also leaks into the conduit. Thus only part of the gas flux serves to increase the foam volume, the remainder being accounted for by leakage. After a fountaining phase, no foam remains at the roof. Thus leakage is initially zero and increases with time as the foam builds up (Appendix A). If the gas flux is larger than the critical value, collapse occurs early in this evolution, and hence the total amount of foam leaked is small. This corresponds to the initial phases of the eruption, where therefore the accumulation rate provides a reasonable estimate of the total gas flux. With time the eruption tends toward the critical conditions, as shown by the decrease of the gas volume erupted (Figure 7) and the fact that fire fountaining

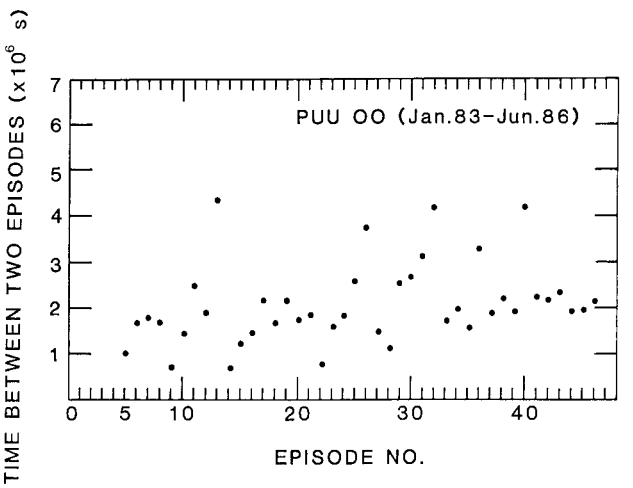

Fig. 8. Repose times between fountaining phases during the 1983–1986 Pu'u O'o eruption (Hawaiian Volcano Observatory data, 1983–1986, courtesy of C. Heliker and G. Ulrich).

eventually stops. Thus foam leakage becomes increasingly important, and the accumulation rate of gas is less than the total gas flux by larger and larger amounts.

We take the erupted gas to be pure CO_2 and compute the corresponding mass at the exit pressure, which must be close to atmospheric [*Wilson and Head*, 1981]. There is also some amount of water, and hence the mass of gas is overestimated. The implied error is small and, in any case, cannot exceed a factor of 2, which is not significant in the present context. The mass accumulation rate of gas at the roof is obtained by dividing this mass by the duration of the preceding repose period t_{1-2}. Figures 9*a* and 9*b* show the results for both the Pu'u O'o and the Mauna Ulu eruptions: it has initially the same order of magnitude of 2–3 $\times$ 10^3 kg/s in both cases and decreases with time. The transition to continuous activity occurs when it drops below values of 90 and 40 kg/s for Pu'u O'o and Mauna Ulu, respectively.

4.4. *Bubble Size and Area of the Chamber Roof*

As explained in section 2.4, the maximum gas volume which can be trapped in a foam layer at a roof of area S is given by

$$V_p = S \frac{4\sigma}{\rho_l g d} \tag{24}$$

where we have used (4) for the critical thickness and bubble diameter d. For a given volume this equation allows the calculation of the bubble diameter as a function of the roof area S. The equation corresponds to the maximum gas volume, and hence we take the largest estimate of 3 $\times$ 10^9 m^3 at atmospheric pressure. At the chamber roof, pressure may range from 5 $\times$ 10^7 to 10^8 Pa, and hence the pocket volume is between 3 $\times$ 10^6 and 6 $\times$ 10^6 m^3. As argued in section 3.1, the chamber location is not known with certainty. The local storage zones at a depth of 2 km below either the summit [*Thurber*, 1987] or the Mauna Ulu and Pu'u O'o vents (Ho-Liu et al., submitted manuscript, 1989), have an area of about 5 km^2. The larger body of magma lying 4 km below the east rift zone occupies an area of at least 30 km^2 (Ho-Liu et al., submitted manuscript, 1989). For the sake of discussion we take bounds of 5 and 30 km^2 and find that the range of bubble diameters is 0.04–0.4 mm (Figure 10). We emphasize that in this problem, all variables are determined in the vicinity of the roof.

An independent approach is to consider how bubbles nucleate and grow in saturated basalt. The bubble size in magma which enters the chamber is determined by the volatile concentration and the ascent velocity [*Sparks*, 1978]. We derive an upper bound by assuming that this ascent velocity is zero, in which case the bubbles rise by their own buoyancy. We use the equations and the computer program written by *Sparks* [1978] and modified by L. Wilson (personal communication, 1988). Each bubble is assumed to be isolated, which is valid at low volume fraction, and grows by diffusion and pressure release. We take a pure CO_2 gas phase with the solubility law of *Stolper and Holloway* [1988]

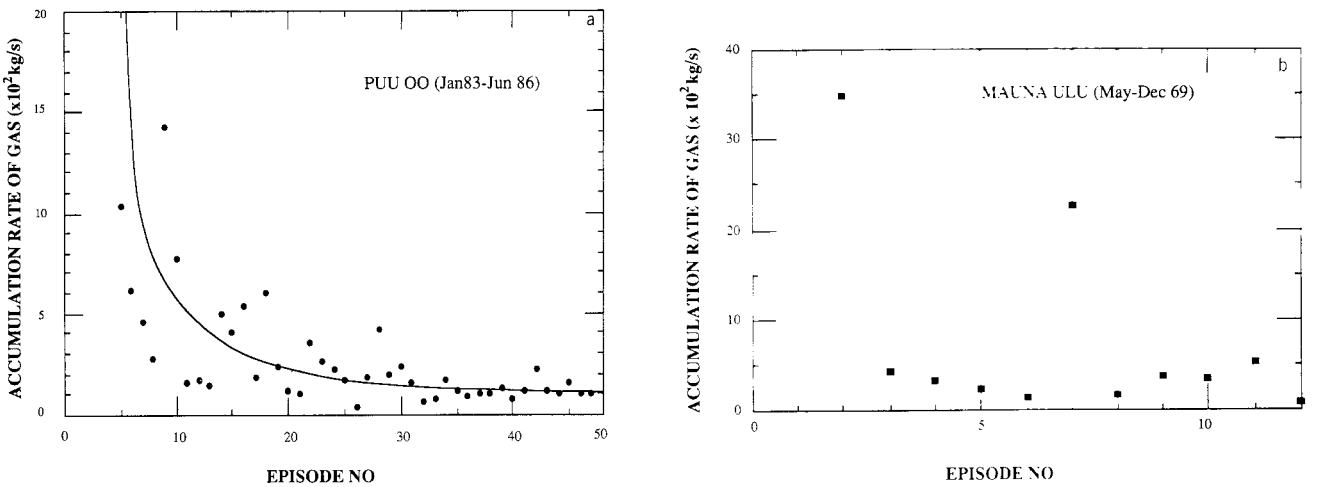

Fig. 9. The accumulation rate of gas at the chamber roof (*a*) for the 1983–1986 Pu'u O'o events and (*b*) for the 1969 Mauna Ulu events. In the initial phases of these eruptions the accumulation rate is close to the gas flux due to bubbles rising toward the chamber roof.

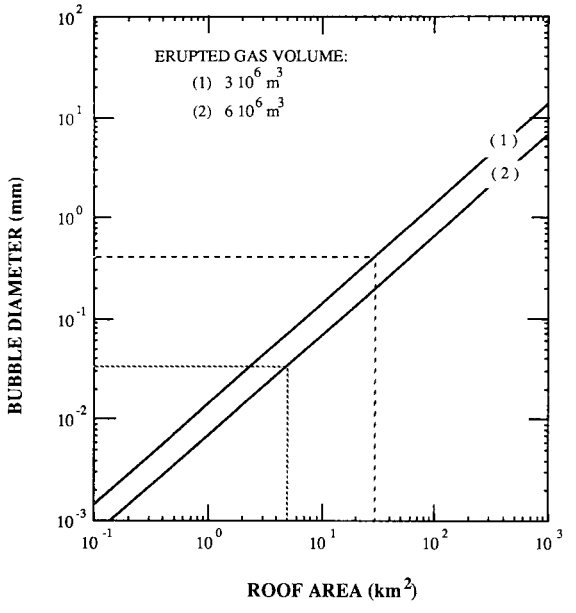

Fig. 10. The bubble size in the Kilauea chamber as a function of roof area (equation (24)) for two estimates of the total gas volume erupted in a fountaining episode. Storage zones imaged by attenuation tomography in the volcanic edifice occupy horizontal areas ranging from about 5 to 30 km^2 (Ho-Liu et al., submitted manuscript, 1989). This range of roof areas leads to bubble sizes in the range of 0.04–0.4 mm.

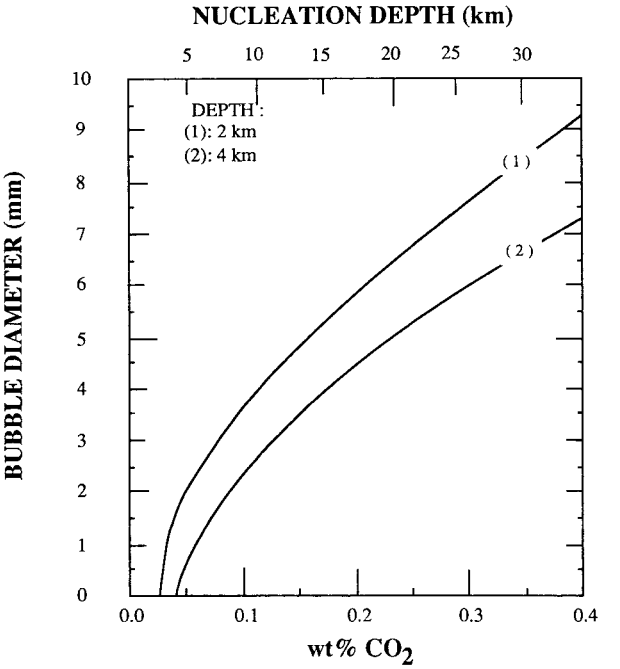

Fig. 11. The maximum diameter of CO_2 bubbles at depths of 2 and 4 km for a stagnant column of saturated basalt. Depending on the CO_2 concentration, bubbles are nucleated at different depths (indicated at the top of the graph) and grow to different diameters. The calculations are made with the computer program by *Sparks* [1978] modified by L. Wilson (personal communication, 1988). In reality, basalt ascends from its mantle source with a finite velocity, and the bubble size must be smaller than shown here.

and use the physical properties given in Table 2. In a magma column extending to an arbitrary depth we compute the bubble size as a function of initial CO_2 concentration, which determines the nucleation depth. Figure 11 shows the results. For the CO_2 concentration of 0.32 wt % [*Greenland*, 1989] the maximum bubble diameter at a depth of 4 km is 6 mm. In a more comprehensive calculation, *Bottinga and Javoy* [1989, 1990] use parental volatile concentrations [*Gerlach and Graeber*, 1985] and an ascent velocity of 2 cm/s and find bubble diameters of about 0.4 mm at the same depth of 4 km. As expected, this diameter is smaller than those of Figure 11. The bubble size will be modified during residence in the chamber. On the one hand, new bubbles may nucleate because crystallization changes the volatile concentration of residual melt [*Tait et al.*, 1989]. On the other hand, some rising bubbles may coalesce before reaching the roof [*Sahagian et al.*, 1989]. In submarine basalts of Kilauea erupted at depths of 4–5 km, where pressure is close to that in shallow magma reservoirs, gas vesicles represent less than 1% by volume and have diameters of about 0.1 mm [*Moore*, 1965]. These values provide lower bounds because bigger bubbles probably escaped upon eruption on the seafloor. We conclude that the bubble size should lie within a range of 0.1–1 mm, which is compatible with that required by the model.

TABLE 2. Physical Properties of Basalts

Physical Parameter	Value	Units
Density	2600	kg m^{-3}
Viscosity	30	Pa s
Surface tension	0.3	kg s^{-2}
Chemical diffusivity of CO_2	1.5×10^{-6}	cm^2 s^{-1}
Solubility constant of CO_2	4.4×10^{-12}	Pa^{-1}

4.5. *Bubble Size and Gas Volume Fraction in the Chamber*

The bubbles are small and rise in a laminar regime. Let α denote the gas volume fraction in magma below the foam. For values of α up to about 60% the rise velocity is [*Wallis*, 1969, pp. 248–252]

$$v_b = (1 - \alpha)\frac{1}{18\mu_l} d^2(\rho_l - \rho_g)g \tag{25}$$

The vertical flux q into the foam due to the rising bubbles, is thus

$$q = \frac{1}{\varepsilon}\alpha v_b \tag{26}$$

The equation for the critical time t_c (equation (22)) is therefore written as

$$\frac{1}{\varepsilon}\alpha(1 - \alpha)\frac{1}{18\mu_l} d^2(\rho_l - \rho_g)gt_c = \frac{4\sigma}{\varepsilon\rho_l g}\frac{1}{d} \tag{27a}$$

This can be rearranged to yield an equation for the bubble diameter:

$$d = \left\{\frac{1}{t_c}\frac{1}{\alpha(1 - \alpha)}\frac{72\sigma\mu_l}{\rho_l^2 g^2}\right\}^{1/3} \tag{27b}$$

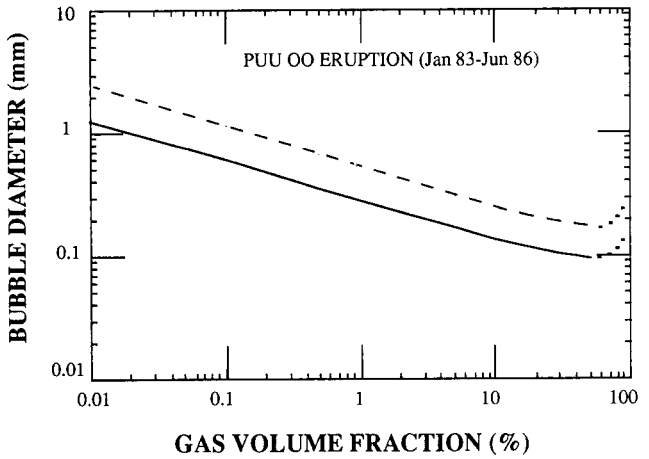

Fig. 12. The bubble size as a function of gas volume fraction α according to equation (27*b*). The bubble size obtained for $\alpha = 50\%$ represents the minimum value (see text). The solid curve corresponds to the best estimate for the critical time t_c, provided by the largest repose time between two fountaining phases (4.3×10^6 s). The dashed curve corresponds to the smallest repose time of 7×10^5 s. Plausible values for α lie in the range of 0.1–10%, and hence the bubble size must be between 0.15 and 0.6 mm.

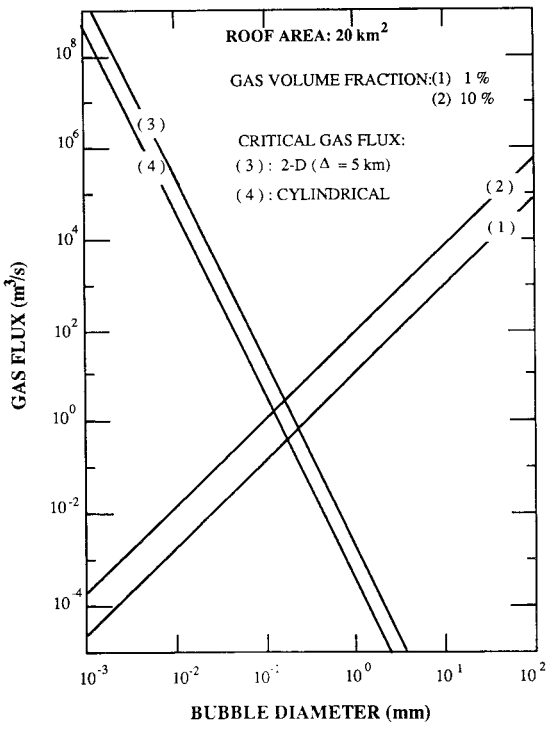

Fig. 13. Gas flux of the chamber roof as a function of bubble size for a roof area of 20 km^2. Curves 1 and 2 correspond to equation (28) for the flux of gas due to rising bubbles for two values of the gas volume fraction α (1% and 10%). Curves 3 and 4 correspond to the critical gas flux below which cyclic activity no longer occurs (equation (20)). The intersection between these two sets of curves allows the determination of the bubble size and the critical gas flux when the eruption changes to a regime of continuous activity.

where we have again neglected the gas density. The interest of this equation is that it depends on the repose time, whose value is easily and reliably measured in the field (Figure 8). Further, it shows that the bubble size is weakly affected by small errors in the various parameters involved. For $\alpha = 50\%$ the gas flux due to rising bubbles is maximum [*Wallis*, 1969, pp. 248–252], which, in the present context, leads to the smallest bubble size. For larger values of α the many bubbles present impede each other and rise with much smaller velocities.

As argued earlier, the repose time can be smaller than the critical time because of partial foam collapse and/or eruption of only a fraction of the gas pocket. Thus the best estimate for t_c is the largest value of 4.3×10^6 s. To illustrate the uncertainty introduced by the observed fluctuations, we also consider the lowest repose time of 7.0×10^5 s. The gas volume fraction in the chamber below the foam is unknown but cannot be varied freely. For example, we assume that the parental magma has a CO_2 concentration of about 0.6 wt % [*Gerlach and Graeber*, 1985] and that the pressure at the chamber roof is 10^8 Pa. At that pressure the CO_2 solubility is about 0.04 wt % [*Stolper and Holloway*, 1988]. If we neglect the effects of separated flow for the gas phase, we find the minimum gas volume fraction of 4%. The calculations of *Bottinga and Javoy* [1989] indicate a value close to 10%. Another constraint may be obtained within the framework of the eruption triggering model of *Tait et al.* [1989]. In this model, fractional crystallization of volatile-saturated melt leads to a pressure increase in the chamber until failure of the edifice. The gas volume fraction stays close to 1% through a large number of successive eruptions. Considering for the sake of discussion a range of 0.1–50%, equation (27*b*) implies that the bubble diameter must be in the range of 0.1–0.6 mm (Figure 12), which is almost identical to the one determined previously. Thus the two independent constraints available are consistent with each other.

As emphasized by Figure 12, the analysis is weakly sensitive to the gas volume fraction, and hence it is possible to use very conservative bounds on this parameter. For the large range of 0.1–50% the two constraints on the gas volume and the intermittency can be combined to yield estimates for both the bubble size and the roof area. The bubble diameter is between 0.1 and 0.6 mm, and the roof area is between 8 and 50 km^2. Tighter bounds for these variables could be derived if the depth of the roof was known. For example, the roof area required by our analysis seems a bit too large for the shallow reservoirs beneath the Mauna Ulu and Pu'u O'o eruptions sites and more compatible with the deep storage zone below the east rift zone (Ho-Liu et al., submitted manuscript, 1989). In the latter case the roof pressure is close to 10^8 Pa, which implies that the pocket volume must be closer to the lowest value of 3×10^6 m^3. In turn, this implies that the roof area and the bubble size should be in the lower end of the quoted ranges.

4.6. *Critical Gas Flux*

The critical gas flux below which cyclic activity is impossible is given by (14) or (17). It is weakly sensitive to the chamber dimensions, and we take a roof area of 20 km^2, in the middle of the required range. For the cylindrical case we take a conduit cross section of 300 m^2 equal to that of the surface vent at Pu'u O'o [*Wolfe et al.*, 1987]. For the two-dimensional case we take Δ to be 5 km. The gas flux is supplied by rising bubbles and hence is expressed as follows:

$$Q = \alpha v_b S \tag{28}$$

where v_b is the bubble rise velocity given by (25). Thus two constraints are available on three variables: the critical gas flux, the bubble size, and the gas volume fraction (Figure 13). Considering the plausible range of 1–10% for α, we find that the bubble size is between 0.1 and 0.2 mm at the lower end of the range found for cyclic activity. The critical gas flux is between 0.5 and 3 m^3/s. For a pure CO_2 gas phase at a pressure of 10^8 Pa this leads to a critical gas flux between values of 10^2 and 10^3 kg/s. This is lower than the values at the start of the eruptions (Figures 9*a* and 9*b*).

4.7. *The 1959 Kilauea Iki Eruption*

This summit eruption showed episodes of fire fountaining lasting from 2 to 30 hours, separated by repose times ranging from 7 hours to 4 days [*Richter et al.*, 1970]. Using again the fountain heights to calculate the exit velocities and the vent cross section of 180 m^2, the gas volume erupted in each episode is between 10^8 and 10^9 m^3. This is slightly smaller than the values found for flank eruptions, implying a smaller roof area for similar values of the bubble size.

5. Discussion

5.1. *Limitations of the Model*

We have investigated a model system which is obviously much simpler than the Kilauea volcano, and it is premature to draw firm conclusions regarding for example the size of the reservoir. The point of our analysis is to show that the model, which reproduces the phenomenology of Hawaiian eruptions, also requires plausible values for key variables. An important result is that within the framework of the model, the two independent quantitative constraints provided by observations are consistent with each other. We now discuss the two critical hypotheses behind our analysis.

The first hypothesis is the presence of a roof where bubbles can accumulate. At Kilauea, chemical evidence shows that magma stays at depth before being erupted and this must occur in some reservoir. The corresponding roof is certainly more complex than in our theory, but this should not affect the key feature of the model, which is the breakdown of foam at a critical thickness. Degassing always leads to the formation of a foam layer whose thickness is determined by a balance between the input of bubbles from below and flow into the conduit. Another roof shape changes the details of this balance, but there will always be a gas flux for which the foam thickness reaches the critical value. As an example, in Appendix B we treat the case of a sloping roof. We note, however, that the seismic data do not support such a case and do indicate the presence of flat interfaces at specific levels in the volcanic edifice [*Ryan*, 1988; *Koyanagi et al.*, 1989, Ho-Liu et al., submitted manuscript, 1989]. Irregularities of the roof surface may also affect the process of foam accumulation and flow. According to the estimates given above for the bubble size the foam thickness is between about 0.2 and 1 m. Wall roughness larger than this over wavelengths of this magnitude would not allow continuous flow toward the conduit. However, two processes act to smooth the roof surface: shear stresses induced by magma flow during repeated eruptions and crust formation due to crystallization. It may also be remarked that local depressions or hollows of the roof would fill with gas, which would have a cushioning effect for foam flow.

The second hypothesis is the separated flow of gas. There are two possibilities for an eruption. One is that there is no injection of magma into the chamber, either because the eruption is triggered by causes internal to the system [e.g., *Tait et al.*, 1989] or because magma injection occurred before. In this case, whatever magma comes out of the chamber is entrained by the erupting gas phase. The other possibility is that an eruption reflects directly the flow of magma from the mantle, and hence there is a background liquid flux through the system. In this case it must be shown that the gas phase has a significant velocity with respect to the liquid phase. This requires a knowledge of the velocity of liquid, i.e., that of reinjection. To determine this, the only way is to use the rates of eruption and edifice deformation together with an assumption on the behaviour of the gas phase. Clearly, the highest possible magma velocity is obtained by neglecting altogether the gas phase. Using this assumption, *Swanson* [1972] estimated that the flux of magma into Kilauea is about 3 m^3/s. This magma enters the bottom of the chamber where it mixes with the resident magma, implying that a large decrease of velocity toward the roof. A rough estimate is obtained by dividing the volume flux by the chamber cross section. For a roof area of 10 km^2 this leads to a magma velocity of 3×10^{-7} m/s. We have found that bubbles probably have diameters of about 0.3 mm. Through a magma of 30 Pa s viscosity these rise with a velocity of 5×10^{-6} m/s, which is much larger than the maximum background magma velocity.

5.2. *Depth of the Magma Chamber*

"Gas piston" activity is due to the ascent and bursting of a gas pocket which is as wide as the conduit [*Swanson et al.*, 1979]. It may be attributed to gas slugs generated by isolated coalescence events in the vicinity of the conduit edge while the foam accumulates [*Jaupart and Vergniolle*, 1988]. As discussed in Appendix C, the ascent velocity of a gas slug is given by [*Wallis*, 1969, p. 285]

$$v_s = 0.345(gD)^{1/2} \tag{29}$$

where D is the conduit diameter. The interesting feature of this equation is that the velocity does not depend on the vertical dimensions of the slug which must vary because of pressure release. Assuming the conduit to be vertical and of constant cross section, Figure 14 shows the depth to the chamber as a function of rise time for such a slug. In the field, lava is seen to rise in the eruption conduit for up to 20 min before bursting occurs [*Swanson et al.*, 1979; *Wolfe et al.*, 1989]. Using bounds of 10 and 20 min for the risetime and conduit diameters of several meters, we find that the chamber roof lies at a depth of a few kilometers. Variations of conduit diameter probably occur over such large distances, but unless they are very large, it is unlikely that the roof is shallower than 1 km.

5.3. *Evolution of Eruption Conditions*

In the framework of this model the transition from cyclic to continuous activity occurs because the gas flux becomes lower than the critical value. This may be due to a decrease of gas flux and/or to an increase of critical value. Rejecting the possibilities that the roof geometry and the magma viscosity change significantly during the eruption, two fac-

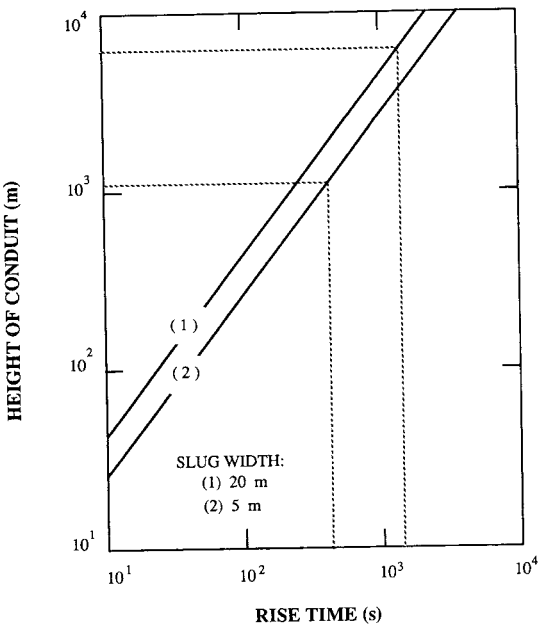

Fig. 14. Height of a vertical eruption conduit as a function of the rise time of gas slugs. Conduit diameters of 5 and 20 m are considered, the latter corresponding to the dimensions of the surface vent of Pu'u O'o [*Wolfe et al.*, 1989]. The risetime is usually estimated to be between 10 and 20 min.

tors remain. One is a decrease of the gas volume fraction, implying a gas flux decrease at constant bubble diameter. The other is a decrease of bubble diameter, which implies both a decreasing flux at constant volume fraction and an increasing critical value. Both factors must be considered simultaneously. At the start of the eruption there is a distribution of bubble sizes in the chamber. With time the different rise velocities will act to develop a stratification in both gas volume fraction and bubble size. One consequence is that the gas flux at the roof may evolve in a complex manner. An analysis of outgassing from a saturated melt along the lines developed by *Toramaru* [1988] would provide a description of the bubble size distribution, which could be tested against the complete eruptive sequence.

5.4. *Implications for the Behavior of Kilauea Volcano*

During the 1959 summit crater eruption, fire fountaining occurred without any variation of the total volume of lava at the surface, indicating that only gas was lost by the system. Flank eruptions are more difficult to interpret because lava is continuously lost as it flows down the volcano slopes. During the 1969–1971 Mauna Ulu eruption, cyclic activity was accompanied by cycles of swelling and deflation of the edifice. Those have been attributed to the temporary storage of magma being fed continuously to the system. This is difficult to explain, all the more as the eruption eventually changed to a regime of continuous effusion where the edifice swelled without deflating. For this second regime the interpretation was that some magma was being stored permanently [*Swanson*, 1972], contrary to what had happened before.

In our model the magma chamber degasses continuously through the eruption, but there are two sources of gas: that in the foam at the roof and that in rising bubbles. At first, the gas flux is above the critical value, implying that the foam is not stable and hence cannot be stored permanently. During a repose period the foam thickens, and hence the volume of stored gas increases. In the laboratory this leads to a rise of liquid level in the conduit. In the volcano this also leads to swelling because the chamber is deformable. Lava effusion ensues at a rate which depends on the combined effects of gas accumulation and chamber expansion. In turn, the accumulation rate of gas at the chamber roof depends on the combined effects of input from below and leakage into the conduit, as already discussed in section 4.3. Through a repose period, leakage increases from an initial value of zero (Appendix A), and hence the accumulation rate of gas decreases. When collapse occurs, the foam releases its gas and the edifice deflates. As the eruption proceeds, the gas flux eventually becomes below critical. This marks the transition to continuous activity, where the foam is stable and hence contributes a permanent volume in the chamber: the edifice therefore swells without deflating. In this case, foam leakage into the conduit is steady, balancing the total gas flux from the chamber interior and following its long-term evolution.

In a general way the presence of a foam layer at the roof may explain other events experienced by the volcano. For example, during the Mauna Ulu eruption, on August 4, 1969, after the sixth episode of fountaining, the Alae lava lake which had been filled drained suddenly. The volume of lava lost in this event was only partially recovered in an ensuring outflow. *Swanson et al.* [1979, p. 18] concluded that about 7.5×10^6 m^3 of lava was added to the rift zone in deep storage. However, they also remarked that this event did not exhibit the characteristics of magma injection. Our explanation is that a volume of gas was lost, replaced by lava draining back into the edifice. The fact that this event was sudden rules out the possibility that it was due to a continuous degassing process. A finite volume must have been made available rapidly at depth: in our view, this was achieved by foam breakdown. For the purposes of an illustrative calculation, let us consider that the magma chamber has a horizontal cross section of 10 km^2 and a thickness of 2 km and hence a volume of 2×10^{10} m^3. The "lost" volume of 7.5×10^6 m^3 represents a tiny proportion of about 0.0004 of that total volume. This rough calculation emphasizes that an eruption is sensitive to the small volume of gas contained in the chamber.

6. CONCLUSION

We have presented a simple model based on the dynamics of degassing in a reservoir which empties into a narrow conduit. The observed behavior of the laboratory analog is similar to that of Kilauea. In this model, gas accumulation takes place at depth. The critical requirement is the presence of a roof or, more generally, some "collection" zone where gas bubbles can accumulate. According to the quantitative analysis the necessary area is between 8 and 50 km^2, which points to the deep storage zone detected at a depth of about 4 km below the east rift zone (Ho-Liu et al., submitted manuscript, 1989). The other requirement of this model is that close to the chamber roof, the bubble size must be a few tens of millimeters. This is close to values obtained in theoretical models of bubble nucleation and growth as well

as to values observed in deep submarine basalts. The model is idealized, and additional tests must be made to assess its applicability to specific eruptions of Kilauea volcano. Measurements of the composition of gases erupted by fire fountains would be useful. Also, a study of the dynamics of the eruption of large gas pockets in magma-filled conduits would allow theoretical predictions of the lava discharge rate and hence a comparison with field data.

The analysis indicates that the volume fraction of gas in the chamber is at least 1%. The presence of a gas phase in such proportions poses the following problem. The total volume of melt expelled during a single eruption represents a small fraction of the volume of Kilauea's storage zones, typically less than 1%. Thus variations in the amount of gas present at depth imply volume variations which may not be negligible in comparison. In other words, the volume (or mass) budget of an eruption cannot be made without taking into account the gas phase explicitly.

APPENDIX A: THE FLUX OF FOAM OUT OF THE ROOF

At time $t = 0$ when the foam begins to accumulate, flow is initially confined to the vicinity of the conduit (Figure 6*a*). In the two-dimensional case it is possible to write an analytical solution [*Jaupart and Vergniolle*, 1989], such that

$$h(x, t) = qtH(\eta) \tag{A1a}$$

where η is a similarity variable defined as

$$\eta = \left(\frac{3\mu_m}{\varepsilon\rho_l g q^3}\right)^{1/2} \frac{x}{t^2} \tag{A1b}$$

The flux of foam at the conduit edge is given by

$$\varphi(0, t) = \frac{\varepsilon\rho_l g}{3\mu_m} h^3 \left.\frac{\partial h}{\partial x}\right|_{x=0} \tag{A2a}$$

which is rewritten as

$$\varphi(0, t) = Bq^{5/2}\left\{\frac{\varepsilon\rho_l g}{3\mu_m}\right\}^{1/2} t^2 \tag{A2b}$$

where B is a constant calculated by numerical integration to be equal to 0.488. Equation (A2*b*) shows that the foam flux out of the roof is finite and further that this flux increases with time. The similarity solution breaks down at large times when flow into the conduit starts affecting the foam at the tank periphery.

If the total gas flux Q is smaller than the critical value, steady state conditions are eventually attained such that flow out of the roof balances exactly the input of bubbles from below. In those conditions the flux of foam is at its maximum, with a value of Q/ε.

If the gas flux is greater than the critical value, foam collapse occurs before steady state at time t_c. Thus the maximum flux of foam is

$$\varphi_m = \varphi(0, t_c) = Bq^{5/2}\left\{\frac{\varepsilon\rho_l g}{3\mu_m}\right\}^{1/2} t_c^2 \tag{A3}$$

which is smaller than Q/ε.

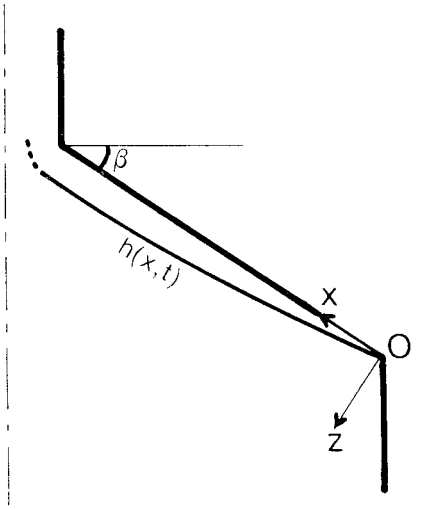

Fig. B1. The case of a sloping roof in two dimensions. The roof makes an angle β with the horizontal and has length L along axis Ox. Oz denotes the coordinate axis perpendicular to the roof.

APPENDIX B: FOAM FLOW ALONG A SLOPING ROOF

The situation investigated is depicted in Figure B1: a roof of length L makes an angle β with the horizontal. We consider the two-dimensional problem, with coordinate system (x, z) attached to the roof. The roof extends over length Δ in the y direction. In the lubrication approximation the equations of motion are as follows:

$$0 = -\frac{\partial P}{\partial x} - \rho_m g \sin\beta + \mu_m \frac{\partial^2 u}{\partial z^2} \tag{B1}$$

$$0 = -\frac{\partial P}{\partial z} + \rho_m g \cos\beta \tag{B2}$$

The difference with the flat roof case is that the driving pressure gradient $\partial P/\partial x$ includes an additional term due to the roof angle. For small values of the angle β this term is small, and hence the physics are not changed appreciably from the flat roof case. For large values of β this term dominates, and the flow of foam is no longer affected by variations of foam thickness (see, for example, the analogous problem tackled by *Huppert* [1982]). We consider the latter case here to show how the situation differs from that investigated in section 2. Integrating (B2), we neglect the term due to the thin foam layer and obtain

$$P(x, h) \approx P_{l0} + \rho_l g(L - x) \sin\beta \tag{B3}$$

where P_{l0} is again the pressure in bulk liquid at the conduit entrance. Substituting this into (B1), we obtain

$$0 = \varepsilon\rho_l g \sin\beta + \mu_m \frac{\partial^2 u}{\partial z^2} \tag{B4}$$

Using the same boundary conditions for velocity (i.e., Figures 10*a*, and 10*b*), we calculate the foam flux per unit width along the y axis:

$$\varphi(x, t) = \int_0^h u(x, z, t)\, dz = \frac{\varepsilon\rho_l g \sin\beta}{3\mu_m} h^3 \tag{B5}$$

Mass conservation then yields

$$\frac{\partial h}{\partial t} = -\frac{\varepsilon \rho_l g \sin \beta}{3\mu_m} \frac{\partial h^3}{\partial x} + q \tag{B6}$$

where q is the input of foam along direction Oz, i.e., normal to the roof:

$$q = Q/\varepsilon 2\Delta L \tag{B7}$$

Using the boundary condition that there is no foam flux at $x = 0$, i.e., at the tank periphery, the steady state foam shape is

$$h(x)^3 = \frac{3\mu_m}{\varepsilon \rho_l g \sin \beta} qx \tag{B8a}$$

The maximum foam thickness for gas flux Q is

$$h_m = \left\{\frac{3\mu_m}{\varepsilon^2 \rho_l g \sin \beta}\right\}^{1/3} \left\{\frac{Q}{2\Delta}\right\}^{1/3} \tag{B8b}$$

There are two important differences with the flat roof case. The maximum foam thickness is reached close to the conduit instead of the tank periphery. Also, the functional dependence of the foam thickness on the gas flux and the foam viscosity is changed. However, for the purposes of the present study the key effect is preserved: the foam thickness increases as a function of gas flux.

Appendix C: The Ascent Velocity of Gas Slugs

The ascent velocity of a gas slug in a cylindrical conduit is determined by three dimensionless parameters [*Wallis*, 1969, p. 285]:

$$\frac{\rho_l v_s^2}{Dg(\rho_l - \rho_g)} \qquad \frac{v_s \mu}{D^2 g(\rho_l - \rho_g)} \qquad \frac{\sigma}{D^2 g(\rho_l - \rho_g)}$$

When the slug is large enough, it rises in an inertial regime where the melt viscosity and surface tension play no role. The ascent velocity is then determined by the first of these three dimensionless numbers, and hence

$$v_s = K\{gD\}^{1/2} \tag{C1}$$

where the constant K takes a value of about 0.345. To verify that the slug does rise in this regime, the Froude number Fr must exceed a value of about 300 and the Eotvos number Eo must be larger than 100. Using (C1) for the ascent velocity, these two dimensionless numbers are written

$$Fr = [D^3 g(\rho_l - \rho_g)\rho_l]^{1/2}/\mu \tag{C2a}$$

$$Eo = D^2 g(\rho_l - \rho_g)/\sigma \tag{C2b}$$

For Hawaiian basalt and $D = 10$ m, $Fr = 2.7 \times 10^4$, and $Eo = 6.8 \times 10^6$. Hence equation (C1) does apply.

Acknowledgments. One of us (S.V.) spent two months at the University of Hawaii (Department of Planetary Geosciences) and at the Hawaiian Volcano Observatory and thanks all the people involved for their kindness and hospitality. This study would not have been possible without the help of the following persons. Robert Koyanagi, Thomas Wright, and Lionel Wilson were always willing to help and gave of their time generously. Christina Heliker provided the essential Pu'u O'o data that she collected with George Ulrich. Stephen Sparks and Lionel Wilson allowed us to use their bubble growth program. Alfred Anderson, Bruce Marsh, Stephen Tait, and Lionel Wilson made very detailed comments and criticisms on the original manuscript. This is contribution CNRS-INSU-DBT (thème instabilités) 140.

References

Batchelor, G. K., *An Introduction to Fluid Dynamics*, 615 pp., Cambridge University Press, New York, 1967.

Beckett, P. M., and G. Poots, Laminar film condensation on horizontal flat plates, *Mech. Res. Commun.*, *2*, 61–66, 1975.

Bottinga, Y., and M. Javoy, MORB degassing: Bubble growth and ascent, *Chem. Geol.*, in press, 1989.

Bottinga, Y., and M. Javoy, Mid-ocean ridge basalt degassing: Bubble nucleation, *J. Geophys. Res.*, in press, 1990.

Burnham, C. W., The importance of volatile constituents, in *The Evolution of Igneous Rocks*, edited by H. S. Yoder, pp. 439–482, Princeton University Press, Princeton, N. J., 1979.

Casadevall, T. J., and D. Dzurisin, Intrusive rocks of Kilauea caldera, *U.S. Geol. Surv. Prof. Pap.*, *1350*, 377–394, 1987.

Garcia, M. O., and E. W. Wolfe, Petrology of the erupted lava, The Puu Oo Eruption of Kilauea Volcano, Hawaii: Episodes 1 Through 20, January 3, 1983, Through June 8, 1984, edited by E. W. Wolfe, *U.S. Geol. Surv. Prof. Pap.*, *1463*, 127–143, 1989.

Gerlach, T. M., The interpretation of volcanic gas data from tholeiitic and alkaline mafic lavas, *Bull. Volcanol.*, *45*, 235–244, 1982.

Gerlach, T. M., and E. Graeber, Volatile budget of Kilauea volcano, *Nature*, *313*, 273–277, 1985.

Greenland, L. P., Hawaiian eruptive gases, *U.S. Geol. Surv. Prof. Pap.*, *1350*, 759–770, 1987.

Greenland, L. P., Gases from the 1983–1984 east-rift eruption, The Puu Oo Eruption of Kilauea Volcano, Hawaii: Episodes 1 Through 20, January 3, 1983, Through June 8, 1984, edited by E. W. Wolfe, *U.S. Geol. Surv. Prof. Pap.*, *1463*, 145–153, 1989.

Greenland, L. P., W. I. Rose, and J. B. Stokes, An estimate of gas emissions and magmatic gas content from Kilauea volcano, *Geochim. Cosmochim. Acta*, *49*, 125–129, 1985.

Harris, D. M., and A. T. Anderson, Concentrations, sources, and losses of H_2O, CO_2 and S in Kilauean basalt, *Geochim. Cosmochim. Acta*, *47*, 1139–1150, 1983.

Head, J. W., and L. Wilson, Lava fountain heights at Pu'u O'o, Kilauea, Hawaii: Indicators of amounts and variations of exsolved magma volatiles, *J. Geophys. Res.*, *92*, 13,715–13,719, 1987.

Hoffman, J. P., Geodetic modeling of the local Pu'u O'o reservoir, Kilauea, Hawaii: From June 1984 to January 1986, *Eos Trans. AGU*, *69*, 1502–1503, 1988.

Huppert, H. E., Flow and instability of a viscous current down a slope, *Nature*, *300*, 427–429, 1982.

Jaupart, C., and S. Vergniolle, Laboratory models of Hawaiian and Strombolian eruptions, *Nature*, *331*, 58–60, 1988.

Jaupart, C., and S. Vergniolle, The generation and collapse of a foam layer at the roof of a basaltic magma chamber, *J. Fluid Mech.*, *203*, 347–380, 1989.

Khitarov, N. I., Ye. B. Lebedev, A. M. Dorfman, and N. Sh. Bagdasarov, Effects of temperature, pressure and volatiles on the surface tension of molten basalt, *Geochem. Int.*, *16*, 78–86, 1979.

Klein, F. W., R. Y. Koyanagi, J. S. Nakata, and W. R. Tanigawa, The seismicity of Kilauea's magma system, *U.S. Geol. Surv. Prof. Pap.*, *1350*, 1019–1186, 1987.

Koyanagi, R. Y., J. T. Unger, E. T. Endo, and A. T. Okamura, Shallow earthquakes associated with inflation episodes at the summit of Kilauea volcano, Hawaii, *Bull. Volcanol.*, *39*, 621–631, 1976.

Koyanagi, R. Y., W. R. Tanigawa, and J. Nakata, Seismicity associated with the eruption, The Puu Oo Eruption of Kilauea Volcano, Hawaii: Episodes 1 Through 20, January 3, 1983, through June 8, 1984, edited by E. W. Wolfe, *U.S. Geol. Surv. Prof. Paper*, *1463*, 183–236, 1989.

Moore, J. G., Petrology of deep-sea basalt near Hawaii, *Am. J. Sci.*, *263*, 40–52, 1965.

Murase, T., and A. R. McBirney, Properties of some common igneous rocks and their melts at high temperatures, *Geol. Soc. Am. Bull.*, *84*, 3563–3592, 1973.

Princen, H. M., Highly concentrated emulsions, 1, *J. Colloid Interface Sci.*, *71*, 55–66, 1979.
Richter, D. H., J. P. Eaton, K. J. Murata, W. U. Ault, and H. L. Krivoy, Chronological narrative of the 1959–60 eruption of Kilauea volcano, Hawaii, *U.S. Geol. Surv. Prof. Pap.*, *537*, 1970.
Ryan, M. P., The mechanics and three-dimensional internal structure of active magma systems: Kilauea volcano, Hawaii, *J. Geophys. Res.*, *93*, 4213–4248, 1988.
Ryan, M. P., R. Y. Koyanagi, and R. S. Fiske, Modeling the three-dimensional structure of macroscopic magma transport system: Application to Kilauea volcano, Hawaii, *J. Geophys. Res.*, *86*, 7111–7129, 1981.
Sahagian, D. L., A. T. Anderson, and B. Ward, Bubble coalescence in basalt flows: Comparison of a numerical model with natural examples, *Bull. Volcanol.*, *52*(1), 49–56, 1989.
Shaw, H. R., T. L. Wright, D. L. Peck, and R. Okamura, The viscosity of basaltic magma: An analysis of field measurements in Makaopuhi lava lake, Hawaii, *Am. J. Sci.*, *266*, 225–264, 1968.
Sparks, R. S. J., The dynamics of bubble formation and growth in magmas: A review and analysis, *J. Volcanol. Geotherm. Res.*, *3*, 1–37, 1978.
Stolper, E., and J. R. Holloway, Experimental determination of the solubility of carbon dioxide in molten basalt at low pressure, *Earth Planet. Sci. Lett.*, *87*, 397–408, 1988.
Swanson, D. A., Magma supply rate at Kilauea volcano 1952–1971, *Science*, *175*, 169–170, 1972.
Swanson, D. A., D. B. Jackson, R. Y. Koyanagi, and T. L. Wright, The February 1969 east rift eruption of Kilauea volcano, Hawaii, *U.S. Geol. Surv. Prof. Pap.*, *891*, 1976.
Swanson, D. A., W. A. Duffield, D. B. Jackson, and D. W. Peterson, Chronological narrative of the 1969–1971 Mauna-Ulu eruption of Kilauea volcano, Hawaii, *U.S. Geol. Surv. Prof. Pap.*, *1056*, 59 pp., 1979.
Tait, S. R., C. Jaupart, and S. Vergniolle, Pressure, gas content and eruption periodicity of a shallow crystallising magma chamber, *Earth Planet. Sci. Lett.*, *92*, 107–123, 1989.
Thurber, C. H., Seismic structure and tectonics of Kilauea volcano, *U.S. Geol. Surv. Prof. Pap.*, *1350*, 919–934, 1987.
Toramaru, A., Vesiculation process of magma and eruption parameters, in *Proceedings of the Kagoshima International Conference on Volcanoes*, pp. 48–50, National Institute for Research Advancement, Tokyo, Japan, 1988.
Urbain, G., Y. Bottinga, and P. Richet, Viscosity of liquid silica, silicates and alumino-silicates, *Geochim. Cosmochim. Acta*, *46*, 1061–1072, 1982.
Vergniolle, S., and C. Jaupart, Separated two-phase flow and basaltic eruptions, *J. Geophys. Res.*, *91*, 12,842–12,860, 1986.
Walker, D., and O. Mullins, Jr., Surface tension of natural silicate melts from 1200°–1500°C and implications for melt structure, *Contrib. Mineral. Petrol.*, *76*, 455–462, 1981.
Walker, G. P. L., Three Hawaiian calderas: An origin through loading by shallow intrusions? *J. Geophys. Res.*, *93*, 14,773–14,784, 1988.
Wallis, G. B., *One Dimensional Two-Phase Flow*, 408 pp., McGraw-Hill, New York, 1969.
Wilson, L., Relationships between pressure, volatile content and ejecta velocity in three types of volcanic eruptions, *J. Volcanol. Geotherm. Res.*, *8*, 297–313, 1980.
Wilson, L., and J. W. Head, Ascent and eruption of basaltic magma on the Earth and Moon, *J. Geophys. Res.*, *86*, 2971–3001, 1981.
Wolfe, E. W., M. O. Garcia, D. B. Jackson, R. Y. Koyanagi, C. A. Neal, and A. T. Okamura, The Puu Oo eruption of Kilauea volcano, episodes 1–20, January 3, 1983 to June 8, 1984, *U.S. Geol. Surv. Prof. Pap.*, *1350*, 471–508, 1987.
Wolfe, E. W., C. A. Neal, N. G. Banks, and T. J. Duggan, Geologic observations and chronology of eruptive events, The Puu Oo eruption of Kilauea volcano, Hawaii: Episodes 1 Through 20, January 3, 1983, Through June 8, 1984, Wolfe, E. W., ed., *U.S. Geol. Surv. Prof. Pap.*, *1463*, 1–98, 1989.
Wright, T. L., D. A. Swanson, and W. A. Duffield, Chemical compositions of Kilauea east-rift lava, 1968–1971, *J. Petrol.*, *16*, 110–133, 1975.

C. Jaupart and S. Vergniolle, Laboratoire de Dynamique des Systemes Geologiques, Universite Paris 7, 4 place Jussieu, 75252 Paris Cedex 05 France.

(Received April 19, 1989;
revised September 19, 1989;
accepted September 19, 1989.)